PCCP

PAPER

View Article Online
View Journal | View Issue

Cite this: *Phys. Chem. Chem. Phys.*, 2018, **20**, 30466

Stability of Au_mAg_n ($m + n = 1–6$) clusters supported on a F-center MgO(100) surface†

Fernando Buendía, Jorge A. Vargas and Marcela R. Beltrán *

Received 31st August 2018,
Accepted 12th November 2018

DOI: 10.1039/c8cp05187a

rsc.li/pccp

A theoretical study has been performed for deposited Au_mAg_n ($m + n = 1–6$) clusters. The combined use of the Mexican Enhanced Genetic Algorithm (MEGA) and Density Functional Theory (DFT) calculations allows us to explore the potential energy surface and therefore, find the global minimum configuration for each composition. We have performed calculations of clusters deposited on defects (oxygen vacancies) known as F centers on MgO (100) surfaces. Our results show interesting differences in the geometries of the clusters upon deposition and as a consequence in their electronic properties. The combination of two metals with different electronegativities creates an inhomogeneous charge distribution on their exposed surface producing good conditions for a catalytic process to take place.

1 Introduction

Gas phase gold clusters are of special interest due to their very peculiar properties, like the observation of planar structures in the small cluster regime (up to 13 atoms depending upon their charge state),[1–9] hollow structure[10–15] and even amorphous-like shape[16–21] due to the gold special electronic configuration and relativistic effects. Their catalytic properties have been widely studied and a characteristic odd–even behavior has been observed in many studies.[22,23]

On the other hand, silver clusters have also been intensively studied by several groups in the past.[24–26] It is unavoidable to notice the similarities in the electronic configurations between the two of them, and therefore some similarities in their behavior, for example small silver clusters (4–8 atoms) are also bi-dimensional.[27] Catalytic properties have also been found for silver clusters although the amount of published work on the latter is more modest in number.[28,29]

The combination of two elements at the nanoscale offers the opportunity not only to tune their already useful properties by controlling their size and composition, but it also offers the opportunity to form nano-alloys that sometimes do not exist at the macro-scale.[25,30–37] This has proved to be particularly useful to obtain better candidates for catalysis. Such is the case of the recently proposed AuRh nano-alloy.[38–41]

Another possibility for studying matter at the nanoscale can be achieved either by adding molecules to the cluster surfaces (functionalizing them)[42] or by depositing them on a non-reactive metal oxide surface.[27,36,43–48] These processes add stability, but the cluster geometries are rearranged and with it, their properties may change. Beyond that, it is known that defects on the surface anchor the cluster to it, avoiding the agglomeration process; this maintains the clusters in specific sizes. Several studies either of gold or silver deposited clusters find that their catalytic properties are maintained.[43,49–55]

The aim of this work is to study structural and electronic changes varying the Au/Ag ratio concentration after deposition. A combination of Density Functional Theory (DFT) with a Genetic Algorithm (GA) has been sucessfully used to find the global minimum configurations in previous works.[56] This methodology is in fact similar to the ones previously detailed in ref. 4 and 5.

In the next section, we briefly discuss the details of both the DFT and GA methods used in this work. In Section 3, we present and discuss structural and electronic Au_mAg_n ($m + n = 1–6$) clusters supported on a defective MgO(100) surface (where a global minimum search is performed over the MgO surface). Finally, we present the conclusions of this work.

2 Methodology

This study has been done applying a genetic algorithm code called the Mexican Enhanced Genetic Algorithm (MEGA),[56] which runs in combination with a plane wave DFT calculation: the Vienna ab initio simulation package (VASP)[57] to perform the minimizations. We employed PBEsol as the exchange and correlation functional, which is known to improve the accuracy when dealing with a solid.[58] The plane wave energy cut-off has been taken at 400 eV for an adequate convergence. Methfessel–Paxton smearing, with a sigma value of 0.01 eV, was implemented

Instituto de Investigaciones en Materiales, Universidad Nacional Autónoma de México, Circ. ext. s/n Apdo. Postal 70-360, C.P. 04510, México D.F., Mexico. E-mail: mbeltran@unam.mx; Tel: +52 5556224624

† Electronic supplementary information (ESI) available. See DOI: 10.1039/c8cp05187a

to improve the SCF convergence of metallic systems. Gamma point calculations were performed. The use of this methodology has given good results in similar systems in earlier publications.[40,59] The initial population of the pool is generated through the minimization of random structures. Once an initial pool has been reached, the algorithm applies mate or mutation operations on the pool structures and relaxes them with VASP to sample selectively the complex potential energy surface. The mate operator takes a pair of clusters from the pool through roulette-wheel selection where the lowest-energy minima within the pool have higher probabilities to be selected. An offspring is then produced through single-point, weighted crossover, carried out according to the Deaven and Ho cut and splice method.[60] For the mutations, MEGA has several operators implemented whose efficiency varies with the type of system it is working on, as it is detailed in previous work.[56] For small bimetallic clusters the "homotop" mutation (swapping the type of a pair of atoms) has been proved to be very efficient to find the lowest-energy structure, while for the mono-metallic clusters the mutations called "move" (a slight random displacement of atoms) and "rotate" (rotation of a few atoms with respect to the rest around a random axis) were used. 80% of the generated clusters were obtained by the mate operator and the remaining 20% were obtained through the corresponding mutation operators. Once the offspring is relaxed, and if the obtained energy is below the highest energy of the clusters in the current pool, MEGA carries out a similarity test to avoid equivalent geometries in the pool. Again, there are different options for the similarity test implemented in MEGA to deal with different kinds of systems. For the small bimetallic clusters studied here, the simplest and fastest option works pretty well. It is just a term-by-term comparison between the ordered and labeled lists with all the interatomic distances of two structures. The similarity test allows MEGA to obtain not only the lowest-energy structure efficiently, but also the isomers close in energy to it. In fact, the algorithm stops when the 5 lowest-energy structures in the pool do not change in 30 steps, which was proven to be adequate for the sizes studied here. MEGA can be used on clusters in the gas phase as well as when supported on a surface. This last possibility is important, because the clusters generated on the surface are even lower in energy than those obtained in the gas phase deposited on every possible facet. This methodology can also simulate the agglomeration process on a substrate.

Our gas phase initial pool consisted of 10 configurations, while for the supported clusters, 15 initial configurations were considered. The calculations have been performed within a cubic supercell leaving at least 10 Å of space between them to avoid cluster–cluster interactions. For the supported systems the clusters were laid onto a $6 \times 6 \times 3$ slab of a MgO(100) surface with a defect on it (an oxygen vacancy, otherwise known as an F-center). 14.7 Å of vacuum between slabs in the z-direction is considered. A convergence study of both geometry and energy observed only small differences ($\Delta x < 2\%$) when the slab is increased, which have been chosen to be ignored for practical purposes. So, only three MgO atomic layers have been taken into account. The approximation employed to calculate the charge transferred is Bader analysis, which is based on the atoms in molecules theory.[61] The spd- and site character of the wave-function for each band was obtained by projecting the orbitals onto spherical harmonics that are non-zero within spheres of the Wigner–Seitz radius around each ion.

The binding energies have been calculated as follows:

$$E_{\mathrm{b}} = -\left[\frac{E_{\mathrm{Au}_m\mathrm{Ag}_n} - \left(mE_{\mathrm{Au}} + nE_{\mathrm{Ag}}\right)}{N}\right], \qquad (1)$$

where $E_{\mathrm{Au}_m\mathrm{Ag}_n}$ is the total energy of the $\mathrm{Au}_m\mathrm{Ag}_n$ cluster and E_{Au} and E_{Ag} are the energies of single, spin-polarized Au and Ag atoms, and N is the total number of atoms.

The energies, E_{ads}, of the surface-supported global minima were calculated as:

$$E_{\mathrm{ads}} = -\left[E_{\mathrm{slab+Au}_m\mathrm{Ag}_n} - \left(E_{\mathrm{slab}} + E_{\mathrm{Au}_m\mathrm{Ag}_n}\right)\right]. \qquad (2)$$

We have used the excess energy (Δ) to determine the stability of the bimetallic clusters relative to pure gold and silver clusters. This quantity is defined as:

$$\Delta E = -\{E(\mathrm{Au}_m\mathrm{Ag}_n) - [(n/N)E(\mathrm{Au}_N) + (m/N)E(\mathrm{Ag}_N)]\}, \qquad (3)$$

where $N = m + n$. The physical meaning of this value is easy to understand, it is the energy of the mixed cluster with respect to pure clusters of the same size; a positive value of Δ implies favorable mixing.[59]

The fragmentation energies are defined as follows:

$$E_{\text{frag-Au}} = -\{E(\mathrm{Au}_n\mathrm{Ag}_m) - [E(\mathrm{Au}_{n-1}\mathrm{Ag}_m) - E(\mathrm{Au})]\} \qquad (4)$$

for gold and:

$$E_{\text{frag-Ag}} = -\{E(\mathrm{Au}_n\mathrm{Ag}_m) - [E(\mathrm{Au}_n\mathrm{Ag}_{m-1}) - E(\mathrm{Ag})]\} \qquad (5)$$

for silver.

Notice that the fragmentation energy in this case only considers that a single atom is removed from the cluster; this is to illustrate the stability of a given cluster with respect to its predecessor rather than a complete study of possible fragmentation processes which is not the purpose of this work.

3 Results and discussion

First, we compare the density of states (DOS) as well as the partial density of states (PDOS) of a perfect MgO(100) surface with a defective one (F-center), shown in Fig. 1a and b respectively. Notice in Fig. 1a a wide band around −2 eV corresponding to the O(2p) orbitals and a band gap of 3.3 eV. In the defective surface (Fig. 1b) a peak appears 2.3 eV above the valence band corresponding to the oxygen vacancy, due to the remaining charge in the Mg(3s) orbitals.

Fig. 2a shows an adsorbed Au atom at an oxygen vacancy and in Fig. 2b an adsorbed Ag atom. Their adsorption energies are 3.60 and 2.18 eV respectively, and the charge transferred from the surface towards the metallic atom is: 1.77 e^- and 1.67 e^- respectively. Therefore the ionic character of the binding between the surface and the metallic atom(s) is revealed. The substitutive (Au or Ag) atoms induce a local deformation, however having much larger atomic radii cannot substitute the oxygen, rather

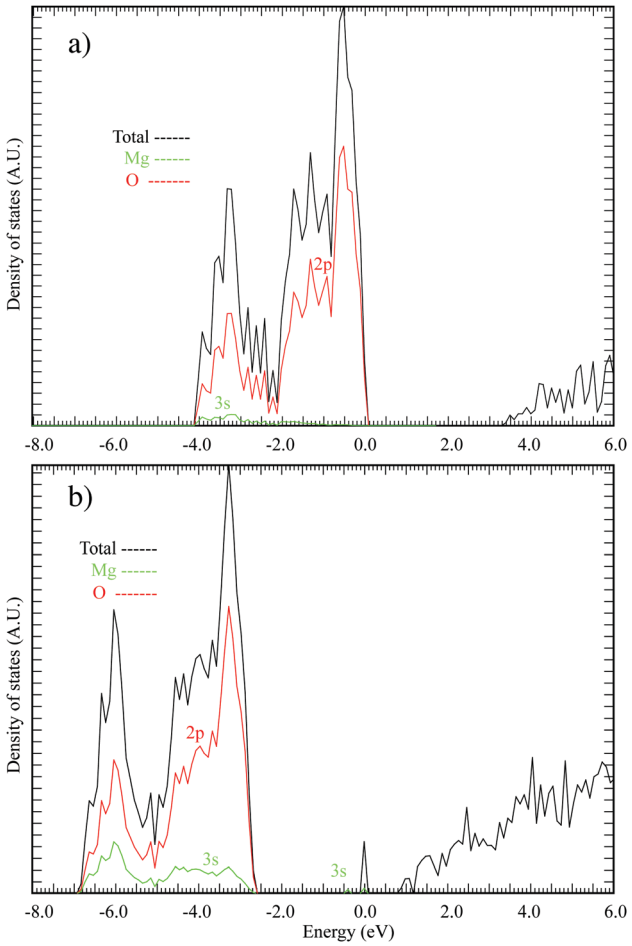

Fig. 1 Magnesium oxide surface DOS and PDOS (top), and magnesium oxide with an oxygen vacancy (F-center) DOS and PDOS (bottom). The Fermi energy has been shifted in order to coincide with 0.0 eV.

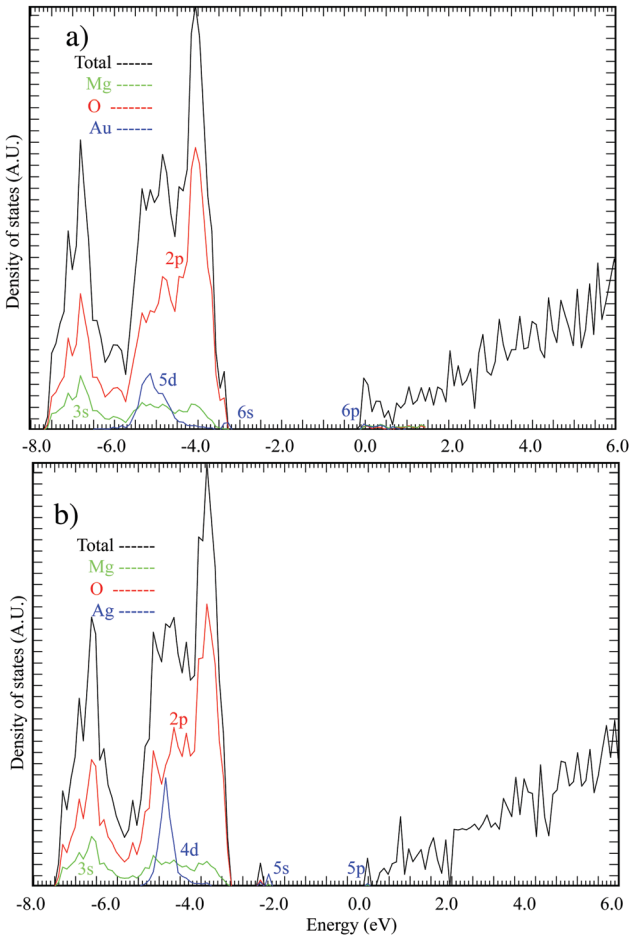

Fig. 2 DOS and PDOS of a gold (a) and a silver (b) atom supported on a defective (F-center) magnesium oxide surface. The Fermi energy has been shifted in order to coincide with 0.0 eV.

both sit above the vacancy but not on top of the surface. A new peak in the DOS located beyond the O(2p) band is generated by the charge transfer from the Mg(3s) to the metallic orbitals; those 2 electrons are transferred towards the *n*s and *n*p orbitals (n = 5 for Ag and n = 6 for Au). For an adsorbed Au atom shown in Fig. 2a a peak with s character is located at a deeper position from the valence band edge (−3.4 eV) when compared with the one associated with the adsorption of an Ag atom (−2.6 eV), see Fig. 2b. This difference in energy is easily explained by the difference in electronegativity between the two metals. A second peak which possesses p character also corresponding to the adsorbed atom lies actually within the conduction band in both cases. In the following subsections we present and discuss the results obtained from a global and unrestricted minimization by means of the methodology DFT-MEGA described in the previous section. For more clarity we only present the lowest energy minimum for each cluster studied.

3.1 Au_n and Ag_n

When either the Au_2 or Ag_2 dimers are supported on a F-center of an MgO surface, both have similar lowest energy isomers (see Fig. 3). One of the atoms substitutes the missing oxygen while the second atom lies on top of a neighboring Mg cation. This provokes a larger charge transfer from the surface towards the clusters (around 0.2 e^-) when we compare it with the monomers. The excess charge belonging to the Au or Ag atom located on the F-center decreases from 1.77 to 1.38 e^- and 1.67 to 1.33 e^- respectively (this can be seen in Fig. 4).

The cluster excess charge enlarges the dimer bond length by 0.17 Å for Au_2 and 0.14 Å for Ag_2, compared with their gas phase bond lengths. In both cases the total adsorption energy is increased with respect to the 1-atom systems (4.41 eV for Au_2 and 2.47 eV for Ag_2); this is shown graphically in Fig. 5. Their corresponding DOS are shown in Fig. 6a and b. The introduction of a second gold atom introduces a 6s and a 5d state at 0.0 and −1.2 eV respectively. Notice how this new d state is much closer to the Fermi energy compared to the d state of the F-center substitutive atom which is located deeper within the band (−3.4 eV). On the other hand, the d state of the second atom lies within the O(2p) band (the Fermi energy has been used as a reference and therefore set at E = 0.0 eV).

Au_3 and Ag_3 are both triangular (see Fig. 3); one atom sits on the vacancy for Au_3 and the two others bond to neighboring Mg atoms. On the other hand, for Ag_3 one atom sits on the vacancy

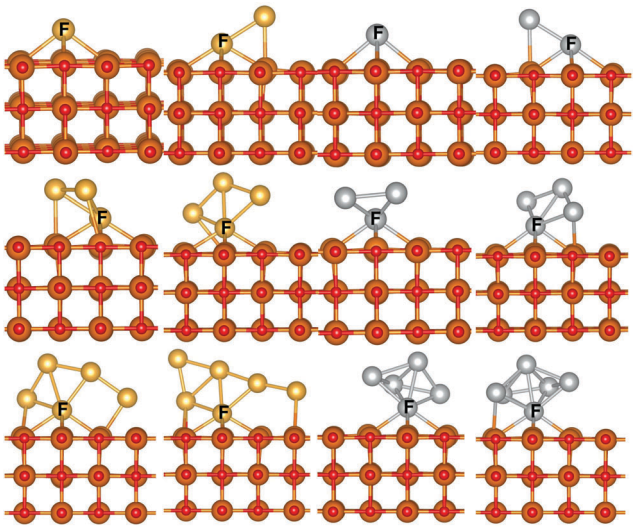

Fig. 3 Geometry of the lowest-energy isomers for Au_n and Ag_n (n = 1–6) supported on a F-center MgO surface.

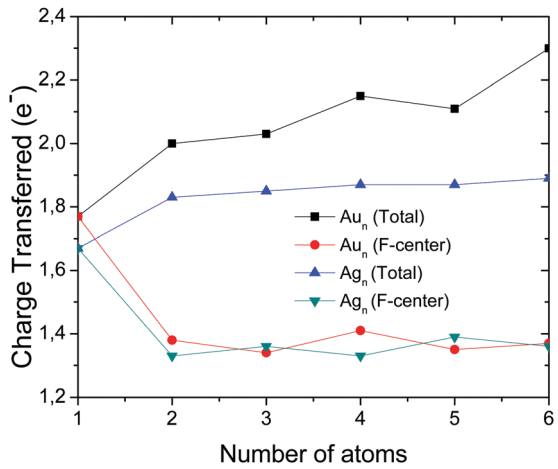

Fig. 4 Charge transfer from the surface towards the Au_n and Ag_n (n = 1–6) clusters supported on a F-center MgO(100) surface.

and the two others are not bonded to the surface. This fact can be explained by the difference in electronegativity between the two elements; Au_3 generates a bigger charge transfer. In both cases the amount of charge transferred towards the atom located on the F-center is similar to the 2 and 1 atom systems. The excess charge that goes to each one of the atoms that are not at the F-center is 0.35 e^- for gold and 0.25 e^- for silver (see Fig. 4).

Au_4 and Ag_4 are distorted rhombuses sitting at an angle; one atom substitutes the vacancy in each case. The farthest atom (from the defect) acts like an electron donor towards the rest of the cluster. For Au_4 the total charge transferred from the surface towards the cluster increases when compared with the previous cases. On the other hand, the charge transfer is similar to the 3 atom cluster for the Ag_4 case. The charge gained by the atom on the F-center is similar to that in previous cases (2 and 3 atoms).

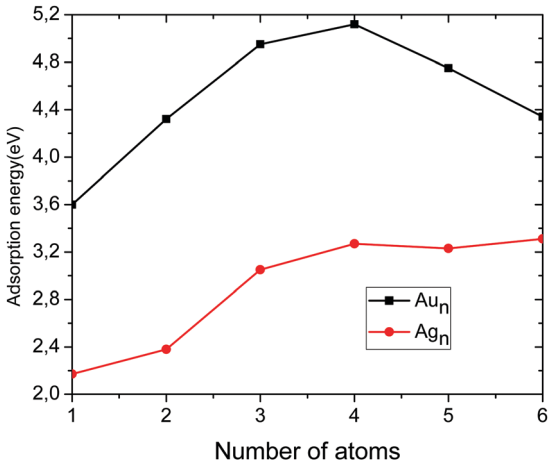

Fig. 5 Adsorption energy of the Au_n and Ag_n (n = 1–6) clusters supported on a F-center MgO(100) surface.

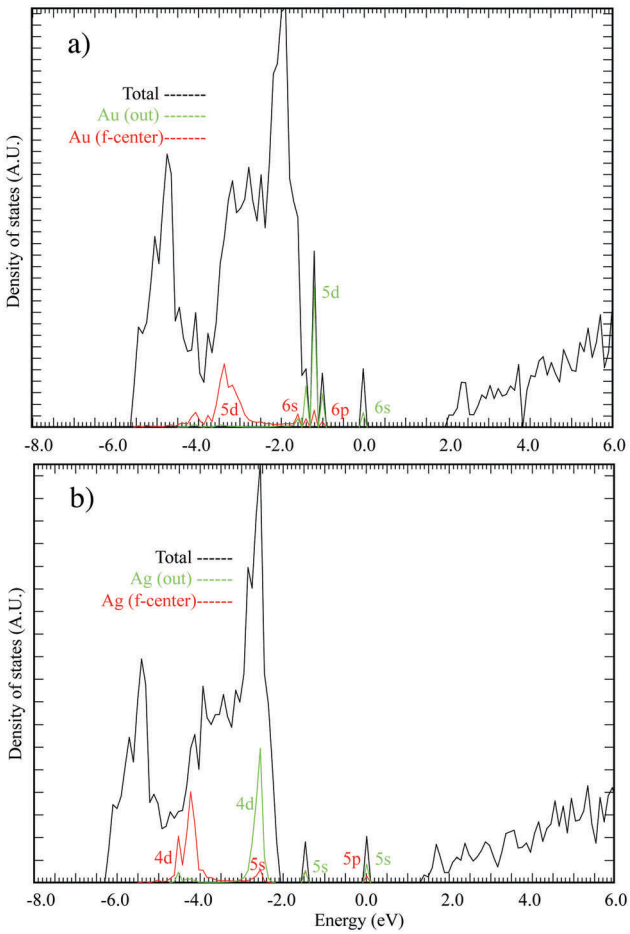

Fig. 6 DOS and PDOS of Au_2 (a) and Ag_2 (b) clusters supported on a F-center magnesium oxide surface. The Fermi energy has been shifted in order to coincide with 0.0 eV.

The monoatomic 5 and 6 gold and silver clusters supported on the surface (Fig. 3) have important geometrical differences. First of all, we notice that our global minimum for Au_6 deposited

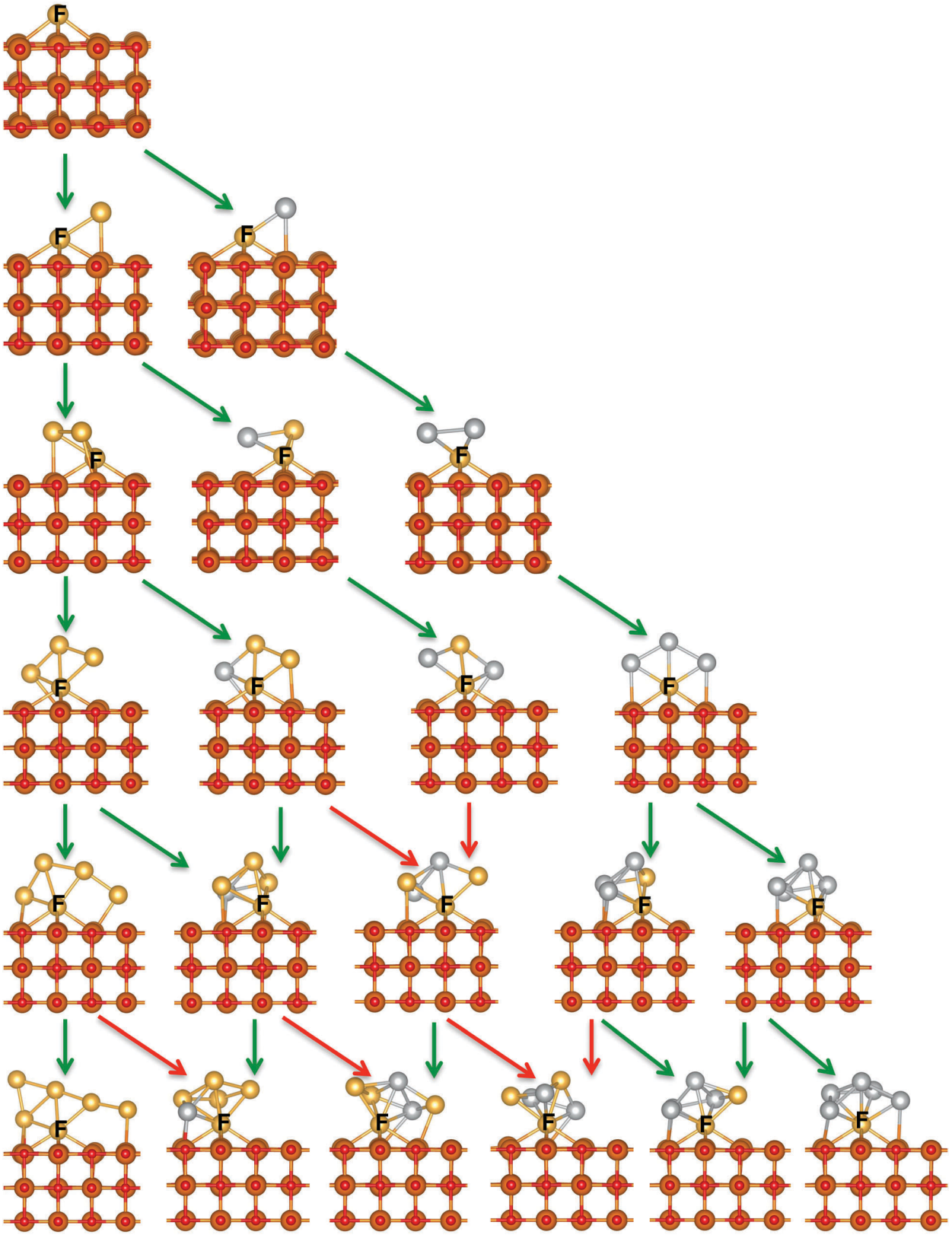

Fig. 7 Lowest energy isomers for Au_nAg_m ($n + m = 1–6$ and $n \geq 1$) supported on a F-center MgO surface marked with a letter F. As atoms are added, green vertical lines represent the addition of gold atoms while diagonal ones indicate the adsorption of Ag atoms. In red are indicated those who require noticeable conformational changes, and may require overcoming an energy barrier. To know if one cluster can be obtained from the adsorption of one atom over a smaller cluster, we compared the bonding network of the clusters. If the bond distances differ by more than 5% one bond can either be broken or can be created generating a new potential energy barrier.

on a F-center is comparable to that obtained by Vilhelmsen *et al.*[47,48] which is also a result of a genetic algorithm global search. The gold clusters are distorted and tend to bond with the Mg cations of the surface. As a consequence the charge transferred towards the cluster increases almost monotonically with size. At the same time the adsorption energy goes down due to the conformational changes with respect to the gas phase. The silver clusters tend to form more compact structures that actually reduce the interaction with the surface. Therefore the total charge transferred towards the cluster is similar to the smaller clusters.

The study of the pure clusters on the defective surface sheds light on the interplay between the ionic bonds with the surface and the covalent bonds created within the cluster. First, pure gold clusters prefer to increase the interaction with the surface dragging charge towards them. On the other hand, silver clusters form more compact structures with covalent bonds within.

The fragmentation energies are bigger for gold than for silver clusters. In both cases, the well documented odd–even behavior characteristic of the gas phase clusters is observed at least in the size range here studied.[22,23] This is due to the addition of an even number of electrons (2 e^-) coming from the F-center.

3.2 Au_nAg_m

For the AuAg dimer, the lowest energy configuration sits the Au atom at the F-center position. When the silver sits at the F-center, the energy is 0.21 eV higher. This difference is due to the electronegativity of the 2 elements. This is explained by the difference in charge transfer towards the "substitutive" atom on the F-center, which in the case of Au is 1.52 e^- and 1.20 e^- for Ag.

The global minima found with MEGA for the 3 atom mixed systems (Au_2Ag and $AuAg_2$) supported on a defective surface have a gold atom at the F-center as shown in Fig. 7 where a frontal view is presented (to add clarity a 45° view for all cases is also shown in the ESI†). On the other hand, the surrounding Ag atoms sit over the neighboring oxygen anions, but for the Au_2Ag case the second Au sits over the Mg cation. The bond increases in both cases due to the charge excess. There is 2.01 e^- for Au_2Ag and 1.94 e^- for $AuAg_2$ charge transferred, but even if these quantities are similar, the inhomogeneity of this is important. The first cluster has one Au atom out of the defect with an excess of 0.56 e^- that could be accessible and useful for possible catalytic purposes, while for $AuAg_2$ the 2 Ag atoms out of the defect only have 0.2 e^- of extra charge (as can be seen in Fig. 8).

The lowest energy minima found in our global search for all 4 atom systems are planar (very similar to the geometries obtained in the gas phase[1–9]). Their structures are depicted in Fig. 7. However, they are not perpendicular to the surface like in the case of the clusters deposited on a perfect MgO surface found in previous studies,[46,59] where the metal on top effect appears. Even for these intermediate sizes, one gold atom is always at the F-center due to its higher electronegativity. Therefore there is a transfer of electronic charge from the surface to the clusters of around 2 e^- dragged from the neighboring

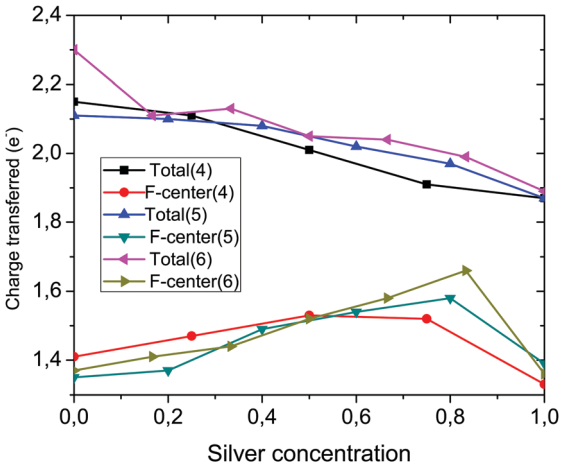

Fig. 8 Total charge transferred (e^-) from the surface to the Au_mAg_n ($n + m$ = 3–6) clusters and charge transferred from the surface to the atom of the cluster located at the F-center position.

Mg cations. Similar to previous cases this excess charge enlarges the Au–Au and Au–Ag distances, especially for the atoms surrounding the defect. The bond lengths of both (Au–Au and Au–Ag) increase on average by 0.15 Å with respect to the gas phase interatomic distances. However the Ag–Ag bond lengths are less increased due to the lesser charge absorbed by the silver atoms.

The increase of silver concentration decreases the total charge transfer, but locally, the charge transferred to the gold atom located at the F-center is actually larger with respect to the rest of the cluster (this can be seen in Fig. 8). For those atoms that are not at the F-center, we observed a little excess of electronic charge that increases with the concentration of gold. Au_3Ag shows the largest amount of charge present in an atom out of the F-center with one Au atom with an excess of 0.43 e^-; this value is even bigger than Au_4. This available extra charge could be useful to catalyze some reaction on its surface. Finally, the excess energy analysis shows that bimetallic clusters are favored over monometallic ones, either in the gas phase or when deposited. However the excess energy is in general lower in the latter case (see Fig. 9). The adsorption energy increases with gold concentration, and for all cases it is larger than the binding energy per atom (see Fig. 10 and 11 respectively). This fact is probably due to the strength of the ionic bonds that the surface forms with the cluster.

The global minima for the supported MgO(100) (F-center) 5 atom-systems are all tridimensional (Fig. 7). The structures of the mixed clusters are similar to that of Ag_5, they form a distorted triangular bi-pyramid, with one of the gold atoms always substituting the missing oxygen atom. There is a considerable charge transfer towards this gold atom, that gives an ionic character to the bonding. The remaining atoms create bonds with the neighboring Mg cations, which also drag a small amount of the excess charge towards them (see Fig. 8). This behavior is similar to the one observed in the 4 atom clusters, and it is due to the higher electronegativity of the gold atom(s). The charge analysis show that Ag atoms acts like donors, increasing the amount of

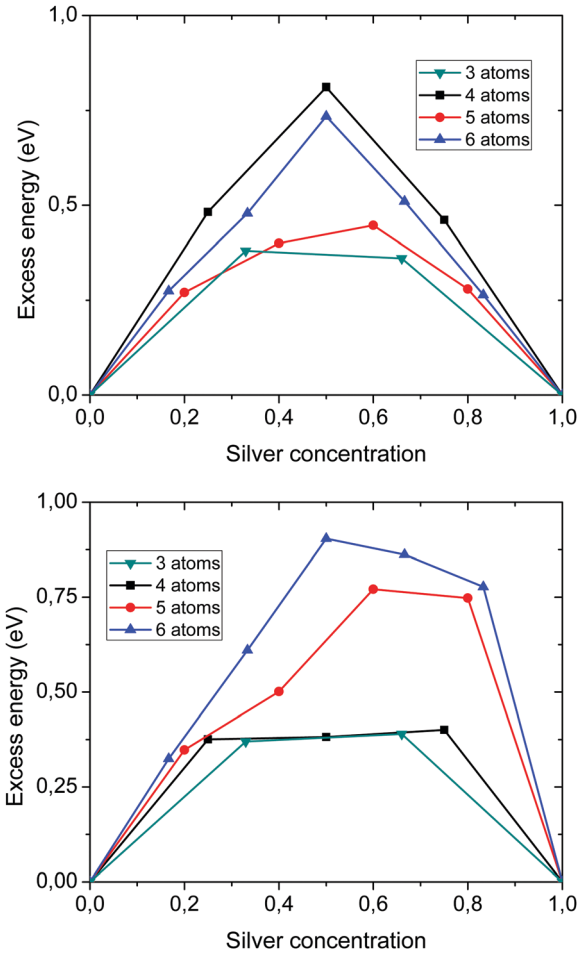

Fig. 9 Excess energy for Au_mAg_n ($m + n$ = 3–6) gas phase clusters (top) and supported on an F center MgO(100) surface (bottom) with respect to Ag concentration.

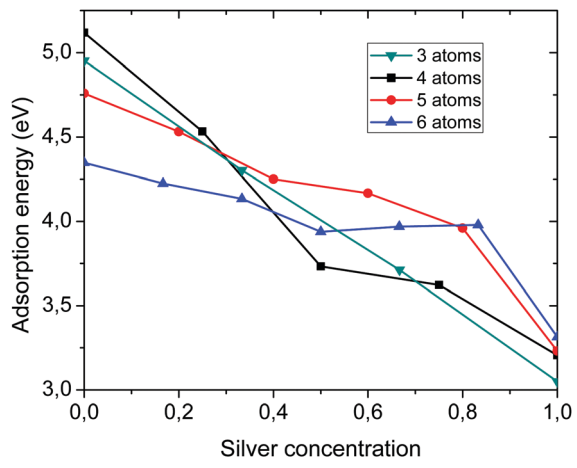

Fig. 10 Adsorption energy for the Au_mAg_n ($n + m$ = 3–6) clusters supported on a F-center MgO(100) surface with respect to Ag concentration.

charge on the gold atoms that are out of the F-center ($\Delta Q \geq 0.4$), favoring the formation of compact structures. Mixed clusters are favored over monometallic ones, and this behavior is enhanced when the clusters are deposited (see Fig. 9). The energy

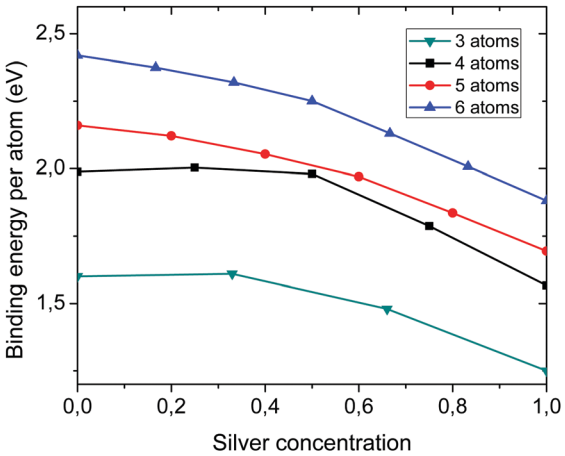

Fig. 11 Binding energy per atom for Au_mAg_n ($n + m$ = 3–6) clusters supported on a F-center MgO(100) surface with respect to Ag concentration.

necessary to remove one Au atom increases from 2.64 eV for Au_5 to 3.64 eV for $AuAg_4$.

The structures of the global minima for Au_6, Au_3Ag_3 and Ag_6 when the clusters are deposited on a MgO perfect surface are presented in Fig. 12 and all of them lie perpendicular to the surface. This is consistent with previous findings.[40,46,59] There is a charge transfer of 0.65 e^- for Au_6, 0.59 e^- for Au_3Ag_3 and 0.32 e^- for Ag_6 from the surface towards the clusters. The charge transfer values are minima due to the electronic stability of the MgO(100) plane surface. However, the high electronegativity of gold attracts a small amount of charge from the surface and allows some interaction between them.

On the other hand, when the clusters are supported on the defect (F-center) the charge transfer is larger (2.30 e^- for Au_6, 2.05 e^- for Au_3Ag_3 and 1.89 e^- for Ag_6, as can be seen in Fig. 7). This fact has also been reported by Vilhelmsen *et al.*[47,48] for the case of pure gold clusters deposited on a MgO(100) F-center surface. The 2 extra electrons located in the defect play a major part. However, Au_6 benefits from a small amount of charge from the Mg atoms which are slightly farther from the defect. The charge on the atoms away from the defect is larger than that of clusters supported on a perfect MgO(100) surface. This shows that most of the excess charge is actually trapped at the gold atom substituting the oxygen vacancy.

The binding energy of the clusters deposited on a perfect MgO(100) surface ranges from 1.60–2.39 eV, but when a defect

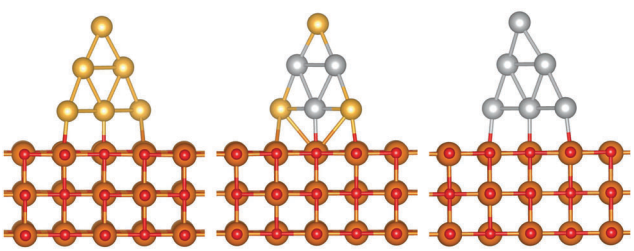

Fig. 12 Geometry of the lowest-energy isomers for Au_6, Au_3Ag_3 and Ag_6 supported on a perfect MgO surface.

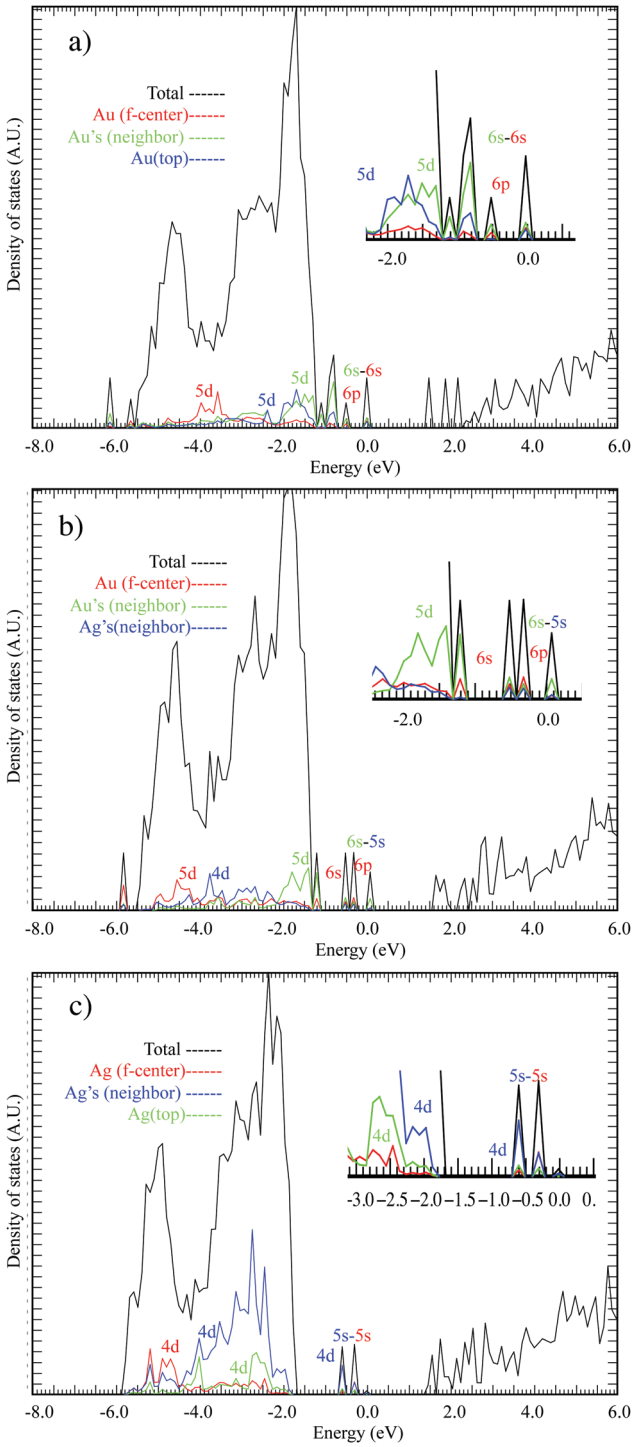

Fig. 13 DOS of (a) Au_6 (b) and Au_3Ag_3 (c) and Ag_6 clusters supported on a F-center MgO(100) surface. The Fermi energy has been shifted in order to coincide with 0.0 eV.

is introduced it is increased (3.31–4.93 eV). This is an important point as it adds stability. The excess energy for the gas phase clusters is positive in all mixed systems, Au_3Ag_3 being the cluster with the largest value. For the clusters on a defective surface we observed that only Au_5Ag is not favored with respect to the monometallic clusters; this is probably due to the high stability of Au_6.

The population of the *n*s and *n*p states of Au_6, Au_3Ag_3, and Ag_6 for the atom located on the F-center is similar, all of them lying close to the Fermi energy, while the *m*d states lie deep within the O(2s) band. On the other hand the position of the *m*d states for the atoms close to the surface varied with the cluster composition (Fig. 13). Finally notice how the silver d-states lie deep within the O(2s) band, but the gold ones are close to the band gap, having the capability to tune the electronic and catalytic behavior.

4 Conclusions

From the structural point of view, we can conclude that the geometry of clusters changes dramatically upon deposition on a defect. On one hand, pure gold clusters generate extended structures over the surface due to the charge transferred, while the silver clusters generate more compact structures due to the preference for forming covalent bonds. On the other hand, the mixed clusters also form compact structures due to the charge transferred from the silver to the gold atoms. Also, due to the covalent character of the cluster at least for the sizes here studied.

We can summarize that the adsorption energy between the cluster and the surface increases with the presence of an oxygen vacancy due to the introduction of ionic character in the bonding. This can reduce the agglomeration process of the clusters in an experimental setting. The stability of these systems is granted as the binding energy is greatly enhanced with the introduction of the defect, avoiding fragmentation.

The observed charge excess remains principally in the atom located at the F-center because the s orbital of this atom shifts deeper within the O(2p) band. For the monoatomic systems, there is no accumulation of charge in any particular site reducing their catalytic capability. On the other hand, in the mixed clusters the electronegativity difference generates charge transfer from the silver to the gold atoms. Therefore, we can foresee very important applications for AuAg mixed clusters in catalysis as the inhomogeneity in the cluster is increased.

The global search we performed by means of MEGA, which is capable of introducing the interaction with a defective surface, proved to be of crucial importance for finding structural changes for supported clusters otherwise impossible to guess.

Conflicts of interest

There are no conflicts to declare.

Acknowledgements

The calculations were performed at the supercomputer Miztli at the supercomputer center in UNAM. We acknowledge the use of the facilities of the IIM (Instituto de Investigaciones en Materiales). We thank Alberto López Vivas and Alejandro Pompa Garcia for their technical support.

References

1 Y. Dong and M. Springborg, *Eur. Phys. J. D*, 2007, **43**, 15–18.
2 R. Wesendrup, T. Hunt and P. Schwerdtfeger, *J. Chem. Phys.*, 2000, **112**, 9356–9362.
3 J. Wang, G. Wang and J. Zhao, *Phys. Rev. B: Condens. Matter Mater. Phys.*, 2002, **66**, 035418.
4 B. Assadollahzadeh and P. Schwerdtfeger, *J. Chem. Phys.*, 2009, **131**, 064306.
5 W. Fa, C. Luo and J. Dong, *Phys. Rev. B: Condens. Matter Mater. Phys.*, 2005, **72**, 205428.
6 P. Gruene, B. Butschke, J. T. Lyon, D. M. Rayner and A. Fielicke, *Z. Phys. Chem.*, 2014, **228**, 337–350.
7 M. A. Flores and E. Menéndez-Proupin, *J. Phys.: Conf. Ser.*, 2016, **720**, 012034.
8 H. Häkkinen and U. Landman, *Phys. Rev. B: Condens. Matter Mater. Phys.*, 2000, **62**, R2287–R2290.
9 M. P. Johansson, A. Lechtken, D. Schooss, M. M. Kappes and F. Furche, *Phys. Rev. A: At., Mol., Opt. Phys.*, 2008, **77**, 053202.
10 S. Bulusu, X. Li, L.-S. Wang and X. C. Zeng, *J. Phys. Chem. C*, 2007, **111**, 4190–4198.
11 W. Fa and J. Dong, *J. Chem. Phys.*, 2006, **124**, 114310.
12 H. Häkkinen, *Chem. Soc. Rev.*, 2008, **37**, 1847–1859.
13 X. Xing, B. Yoon, U. Landman and J. H. Parks, *Phys. Rev. B: Condens. Matter Mater. Phys.*, 2006, **74**, 165423.
14 S. Bulusu, X. Li, L.-S. Wang and X. C. Zeng, *Proc. Natl. Acad. Sci.*, 2006, **103**, 8326–8330.
15 W. Huang, S. Bulusu, R. Pal, X. C. Zeng and L.-S. Wang, *ACS Nano*, 2009, **3**, 1225–1230.
16 M. Ji, X. Gu, X. Li, X. Gong, J. Li and L.-S. Wang, *Angew. Chem., Int. Ed.*, 2005, **44**, 7119–7123.
17 N. Shao, W. Huang, Y. Gao, L.-M. Wang, X. Li, L.-S. Wang and X. C. Zeng, *J. Am. Chem. Soc.*, 2010, **132**, 6596–6605.
18 X. Gu, S. Bulusu, X. Li, X. C. Zeng, J. Li, X. G. Gong and L.-S. Wang, *J. Phys. Chem. C*, 2007, **111**, 8228–8232.
19 S. Bulusu and X. C. Zeng, *J. Chem. Phys.*, 2006, **125**, 154303.
20 D. Tian and J. Zhao, *J. Phys. Chem. A*, 2008, **112**, 3141–3144.
21 I. L. Garzón, M. R. Beltrán, G. González, I. Gutiérrez-González, K. Michaelian, J. A. Reyes-Nava and J. I. Rodrguez-Hernández, *Eur. Phys. J. D*, 2003, **24**, 105–109.
22 A. Prestianni, A. Martorana, F. Labat, I. Ciofini and C. Adamo, *J. Mol. Struct. THEOCHEM*, 2009, **903**, 34–40.
23 C. Zhang, B. Yoon and U. Landman, *J. Am. Chem. Soc.*, 2007, **129**, 2228–2229.
24 Y. Rao, Y. Lei, X. Cui, Z. Liu and F. Chen, *J. Alloys Compd.*, 2013, **565**, 50–55.
25 V. Bonačić-Koutecký, J. Burda, R. Mitrić, M. Ge, G. Zampella and P. Fantucci, *J. Chem. Phys.*, 2002, **117**, 3120–3131.
26 L. F. L. Oliveira, N. Tarrat, J. Cuny, J. Morillo, D. Lemoine, F. Spiegelman and M. Rapacioli, *J. Phys. Chem. A*, 2016, **120**, 8469–8483.
27 C. Bürgel, R. Mitrić and B.-K. Vlasta, *Phys. Status Solidi B*, 2010, **247**, 1099–1108.
28 K.-i. Shimizu, M. Tsuzuki, K. Kato, S. Yokota, K. Okumura and A. Satsuma, *J. Phys. Chem. C*, 2007, **111**, 950–959.
29 L. Jiang and Q. Xu, *J. Phys. Chem. A*, 2006, **110**, 11488–11493.
30 S. Chretien, M. S. Gordon and H. Metiu, *J. Chem. Phys.*, 2004, **121**, 9931–9937.
31 P. Liu, K. Song, D. Zhang and C. Liu, *J. Mol. Model.*, 2012, **18**, 1809–1818.
32 F. Calvo, A. Fortunelli, F. Negreiros and D. J. Wales, *J. Chem. Phys.*, 2013, **139**, 111102.
33 A. Shayeghi, R. Schefler, D. M. Rayner, R. L. Johnston and A. Fielicke, *J. Chem. Phys.*, 2015, **143**, 024310.
34 A. Shayeghi, C. J. Heard, R. L. Johnston and R. Schefler, *J. Chem. Phys.*, 2014, **140**, 054312.
35 J. Sui, X. Wang and P. An, *Comput. Theor. Chem.*, 2014, **1028**, 98–105.
36 S. Heiles, A. J. Logsdail, R. Schafer and R. L. Johnston, *Nanoscale*, 2012, **4**, 1109–1115.
37 G. Rossi, R. Ferrando, A. Rapallo, A. Fortunelli, B. C. Curley, L. D. Lloyd and R. L. Johnston, *J. Chem. Phys.*, 2005, **122**, 194309.
38 F. Buendía, M. R. Beltrán, X. Zhang, G. Liu, A. Buytendyk and K. Bowen, *Phys. Chem. Chem. Phys.*, 2015, **17**, 28219–28227.
39 J.-X. Yang, C. F. Wei and J. J. Guo, *Phys. B*, 2010, **405**, 4892–4896.
40 F. Buendia, J. A. Vargas, M. R. Beltran, J. B. A. Davis and R. L. Johnston, *Phys. Chem. Chem. Phys.*, 2016, **18**, 22122–22128.
41 F. Buendía and R. M. Beltrán, *Eur. Phys. J. D*, 2016, **70**, 1–9.
42 A. M. Joshi, M. H. Tucker, W. N. Delgass and K. T. Thomson, *J. Chem. Phys.*, 2006, **125**, 194707.
43 G. Barcaro and A. Fortunelli, *New J. Phys.*, 2007, **9**, 22.
44 J. Wang, H. Tan, S. Yu and K. Zhou, *ACS Catal.*, 2015, **5**, 2873–2881.
45 A. Kulesza, R. Mitrić and V. Bonačić-Koutecký, *Phys. Chem. Chem. Phys.*, 2012, **14**, 9330–9335.
46 C. J. Heard, S. Heiles, S. Vajda and R. L. Johnston, *Nanoscale*, 2014, **6**, 11777–11788.
47 L. B. Vilhelmsen and B. Hammer, *Phys. Rev. Lett.*, 2012, **108**, 126101.
48 L. B. Vilhelmsen and B. Hammer, *J. Chem. Phys.*, 2014, **141**, 044711.
49 E. C. Tyo and S. Vajda, *Nat. Nanotechnol.*, 2015, **10**, 577–588.
50 P. Ghosh, M. Farnesi Camellone and S. Fabris, *J. Phys., Lett.*, 2013, **4**, 2256–2263.
51 M. Cerbelaud, G. Barcaro, A. Fortunelli and R. Ferrando, *Surf. Sci.*, 2012, **606**, 938–944.
52 A. R. Puigdollers, P. Schlexer and G. Pacchioni, *J. Phys. Chem. C*, 2015, **119**, 15381–15389.
53 M. Amft, B. Sanyal, O. Eriksson and N. V. Skorodumova, *J. Phys.: Condens. Matter*, 2011, **23**, 205301.
54 Z.-K. Han and Y. Gao, *Nanoscale*, 2015, **7**, 308–316.
55 R. Ferrando, G. Barcaro and A. Fortunelli, *Phys. Rev. B: Condens. Matter Mater. Phys.*, 2011, **83**, 045418.
56 J. A. Vargas, F. Buendía and M. R. Beltrán, *J. Phys. Chem. C*, 2017, **121**, 10982–10991.
57 J. Hafner, *J. Comput. Chem.*, 2008, **29**, 2044–2078.
58 J. P. Perdew, A. Ruzsinszky, G. I. Csonka, O. A. Vydrov, G. E. Scuseria, L. A. Constantin, X. Zhou and K. Burke, *Phys. Rev. Lett.*, 2008, **100**, 136406.
59 H. A. Hussein, J. B. A. Davis and R. L. Johnston, *Phys. Chem. Chem. Phys.*, 2016, **18**, 26133–26143.
60 D. M. Deaven and K. M. Ho, *Phys. Rev. Lett.*, 1995, **75**, 288–291.
61 G. Henkelman, A. Arnaldsson and H. Jónsson, *Comput. Mater. Sci.*, 2006, **36**, 354–360.

